

1 **Influence of Warming and Atmospheric Circulation Changes on**
2 **Multidecadal European Flood Variability**

3

4 Stefan Brönnimann,^{1,2,*} Peter Stucki,^{1,2} Jörg Franke,^{1,2} Veronika Valler,^{1,2} Yuri Brugnara,^{1,2} Ralf
5 Hand,^{1,2} Laura C. Slivinski,^{3,4} Gilbert P. Compo,^{3,4} Prashant D. Sardeshmukh,^{3,4} Michel Lang,⁵ Bettina
6 Schaeffli^{1,2}

7

8 ¹ Oeschger Centre for Climate Change Research, University of Bern, Switzerland

9 ² Institute of Geography, University of Bern, Switzerland

10 ³ University of Colorado, CIRES, Boulder, USA

11 ⁴ NOAA Physical Sciences Laboratory, Boulder, USA

12 ⁵ INRAE, Lyon-Villeurbanne, France

13 * corresponding author: stefan.broennimann@giub.unibe.ch

14

15 **Abstract**

16 European flood frequency and intensity change on a multidecadal scale. Floods were more frequent in
17 the 19th (Central Europe) and early 20th century (Western Europe) than during the mid-20th century and
18 again more frequent since the 1970s. The causes of this variability are not well understood and the
19 relation to climate change is unclear. Palaeoclimate studies from the northern Alps suggest that past
20 flood-rich periods coincided with cold periods. In contrast, some studies suggest that more floods
21 might occur in a future, warming world. Here we ~~reconcile the apparent contradiction by addressing~~
22 ~~and quantifying~~ the contribution of atmospheric ~~processes circulation and of warming~~ to multidecadal
23 flood variability. For this, we use long series of annual peak streamflow, daily weather data,
24 reanalyses, and reconstructions. We show that both changes in atmospheric circulation and moisture
25 content affected multidecadal changes of annual peak streamflow in Central and Western Europe over
26 the past two centuries. We find that during the 19th and early 20th century, atmospheric circulation
27 changes led to high peak values of moisture flux convergence. The circulation was more conducive to
28 strong and long-lasting precipitation events than in the mid-20th century. These changes are also partly
29 reflected in the seasonal mean circulation and reproduced in atmospheric model simulations, pointing
30 to a possible role of oceanic variability. For the period after 1980, increasing moisture content in a
31 warming atmosphere led to extremely high moisture flux convergence. Thus, the main atmospheric
32 driver of flood variability changed from atmospheric circulation variability to water vapour increase.

33

34 **1. Introduction**

35 Changes in flood frequency and intensity depend on many factors (Hall, 2014; Tarasova, 2019)
36 including changes in atmospheric processes such as moisture flux, convection, precipitation at
37 different time scales, changes in hydrological processes such as infiltration or overland flow, the
38 seasonal coincidence of snow melt and heavy precipitation, and on human interventions such as river
39 bed and lake regulations, hydropower plants or other hydraulic constructions. Some of these factors
40 are affected by climate change, but also multidecadal variations of climate play a role. During the 19th
41 century, floods were more frequent in Alpine countries (Glaser et al., 2004, 2010; Brázdil et al., 2005;
42 Blöschl et al., 2020, Schmockler-Fackel and Naef, 2010a,b; Himmelsbach et al., 2015; Lang et al.,
43 2016) triggering political discussion that led to legislation on forest conservation and hydraulic
44 engineering (Summermatter, 2005). In contrast, floods were comparably rare in Central Europe in the
45 mid-20th century, a period when large infrastructure projects were planned and carried out (Pfister
46 2009). The causes of this multidecadal flood variability are not well understood. Atmospheric
47 circulation changes played a role (Jacobeit et al., 2003; Mudelsee et al., 2004; Quinn and Wilby, 2013;
48 Brönnimann et al., 2019), but this has not been well quantified. Furthermore, the relation to climate
49 change is unclear. In this paper we analyse multidecadal flood variability in Europe in relation to
50 atmospheric processes and in particular their link to climate change.

51 Better understanding this relation is relevant for assessing future flood risk. ~~In that context, it is~~
52 ~~important to note that For this it is important to settle a long standing controversy: While~~ palaeoclimate
53 studies (Stewart et al., 2011; Glur et al., 2013; Engeland et al., 2020, Wilhelm et al. 2022) from the
54 ~~northern~~-Alps or Norway suggest that past flood-rich periods coincided with cool periods,
55 ~~Conversely,~~ climate projections suggest that with global warming, flood occurrence will increase
56 globally and ~~an increase in flood risk is “very likely” in the majority of regions~~ countries representing
57 70% of the world population (Alfieri et al., 2017; IPCC, 2021). ~~This is because of an increase in heavy~~
58 ~~precipitation due to increased atmospheric moisture, though changes are region-specific and depend,~~
59 ~~among other things, on atmospheric circulation changes~~ (IPCC, 2021). Our paper addresses ~~this~~
60 ~~question~~ effects of atmospheric circulation changes and of climate warming on European floods on a
61 multidecadal scale, following the work of Blöschl et al. (2020), by applying ~~We apply~~ a dynamical
62 perspective to a long period (200 years) that covers both types of flood periods ~~(cold and flood rich,~~
63 ~~warm and flood rich).~~

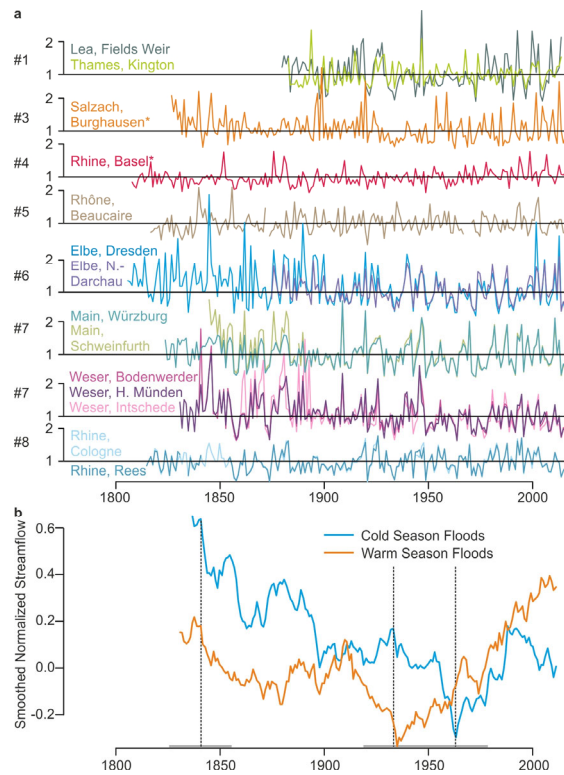
64 In this paper we specifically ~~focus on the atmospheric contribution to flood variability. In particular,~~
65 ~~we~~ explore to what extent atmospheric processes can explain multidecadal variability in flood
66 intensity. We also investigate how the atmospheric contribution can be further partitioned into
67 contributions from circulation changes and moisture changes. To achieve this, we analyze long annual
68 peak streamflow series, daily weather data, reanalyses, and reconstructions.

69

70 **2. Data and Methods**

71 *2.1. Annual peak streamflow series and daily precipitation series*

72 We use annual maximum streamflow from the Global Runoff Data Center (GRDC) from all series in
73 the region 42-60° N, 2° W to 18° E that are at least 110 years long (in 1904-/1905 a network was
74 installed in Switzerland, hence coverage increases; one obviously inhomogeneous series from Sweden
75 was excluded). Note that daily data are not available from this source, hence our focus on annual
76 maximum streamflow. This set was supplemented with two long daily streamflow series from the
77 Rhône (Lang et al., 2016) and Rhine (Wetter et al., 2011), ~~r-This+resultinged~~ in a set of 45 series
78 (Table S1). For comparison, all series were scaled with their ~~1901-2000~~ long-term average. The
79 fourteen longest series are shown in Fig. 1a for illustration. For all further analyses, we normalized the
80 series by fitting a Gamma distribution (Botter et al., 2013) and transforming to the quantiles of a
81 standard normal distribution (we also analysed the raw data, which gave similar results). Since in later
82 steps, series will be aggregated, this transformation ensures that combined series have more similar
83 properties. Both the scaling and the transformation to a normal distribution were performed based on a
84 common reference period comprising all data after 1900. We term these series “flood intensity”,
85 noting that not each annual value would be called a “flood”. For the two daily series, we also analysed
86 the flood frequency (exceedance of the 98th percentile, declustered by combining events up to 3 days
87 apart, see Sect. 2.4). A comparison for 30-yr moving averages is shown in Fig. S2. Note that
88 palaeoclimate studies are often based on events with a longer return period (e.g., 10 years or longer;
89 Wilhelm et al., 2021).



90
 91 **Figure 1. a** Scaled series of annual peak streamflow for the 14 longest series in Central Europe (Table S1,
 92 numbers on the left refer to the regions defined in Sect. 2.2). Stars denote streamflow series with predominantly
 93 summer floods. **b** Normalized series of annual peak streamflow averaged (50% of rivers must have data) for
 94 rivers with predominantly cold-season floods (blue) and warm-season floods (orange), smoothed with a 30-yr
 95 moving average (min. 20 available years) (50% of rivers must have data, first and last 15 years omitted). Dashed
 96 lines with grey bars show the 30-yr intervals chosen for analysis.

97 To each of the streamflow series a daily precipitation record from a neighbouring station was assigned.
 98 For this, we searched GHCN daily (Vose et al., 1992), ECAD (Klein Tank et al., 2002) as well as
 99 series from MeteoSwiss, and selected series that are as long as possible and, if possible, from a
 100 location upstream of the streamflow series (Table S1). Note that in some regions long precipitation
 101 records are sparse, and in some cases the same precipitation record was used for more than one
 102 streamflow record. Furthermore, it should be noted that these series have not been homogenized and
 103 their long-term stability is questionable. Only in one case (Hohenpeissenberg), we accounted for an
 104 obvious inhomogeneity by excluding data prior to 1879. From the precipitation series we calculated
 105 $Rx5day$ and $Rx20day$, *i.e.*, the annual maxima of precipitation sum over periods of 5 and 20 days,
 106 respectively. The latter is used to characterize the seasonality of hydrological preconditions (e.g., soil
 107 saturation) in a catchment, as further discussed in the next section. The former is used as a diagnostic
 108 of flood-propelling events. Previous work (Froidevaux et al. 2015, Brönnimann et al. 2019) has shown

109 [that flood events are mostly affected by precipitation on 3-4 days prior to the event. Although](#)
110 [catchment size varies in our studies, Rx5day is expected to characterize heavy rainfall characteristics](#)
111 [over a large range of catchments.](#)

112 2.2. Regionalisation

113 In a next step, the streamflow series were grouped into regions with hydro-meteorological
114 characteristics as similar as possible using Ward clustering (Ward.D2 in R). We considered the
115 seasonalities of annual maximum streamflow, Rx5day, and Rx20day (i.e., the probability of annual
116 maximum of precipitation over a 5-day window or peak stream flow to fall into a specific month, Fig.
117 S1), the coordinates of the river gauge as well as the coordinates of the precipitation station. The series
118 were standardized and scaled such that streamflow, precipitation, river coordinates, and precipitation
119 coordinates each contributed the same variance. A separation into nine clusters resulted in mostly
120 regionally coherent, non-overlapping clusters. One cluster comprised series from two different
121 catchments (Elbe, Danube) and was correspondingly split and merged with the existing Danube cluster
122 and with an Elbe sub-cluster. Additionally, one river (Ilz) was moved from the Danube cluster
123 (although the Ilz is a tributary of the Danube) to the central Germany cluster as the flood seasonality is
124 clearly distinct from that of the Danube (Fig. S23).

125 Within the Alpine clusters (Rhône, Alpine Rhine, Danube), individual peak streamflow series show
126 strikingly different trends (Fig. 2). Apart from the fact that the flood season changes from summer (in
127 the Alps) to winter (in the lowland) in all three rivers, which is partly reflected in the clustering as the
128 change occurs relatively far away from the Alps, also long-term trends radically change from the Alps
129 to the Alpine foreland. The highest catchments (mean elevation >2000 m asl) in all three regions
130 (Rhône, Porte-Du-Scex; Rhine Domatems; Inn Martinsbruck) show a strong decrease since the early
131 20th century, whereas the long-term evolution further downstream is flat (Rhône, Chancy) or
132 increasing (Rhine, Basel; Danube, Achleiten, Fig. 2). A possible explanation relates to the role of
133 snow processes on high-altitude catchments. Trends could then be due to a superposition of the
134 seasons of snow melt and heavy precipitation in the early 20th century, whereas the two seasons are
135 more separated today (FOEN, 2021). Other explanations include the role of power plants or other
136 hydraulic constructions on the flood regime ([which is studied for the case of Porte-du-Scex, see](#)
137 [Hingray et al. 2010](#)). In any case, since the focus of this study is on atmospheric processes, these rivers
138 might confuse our results and hence we removed five series from the three clusters ([Inn at](#)
139 [Martinsbruck, Rhône at Porte-Du-Scex, and Rhine at Domatems, Neuhausen, and Rekingen](#)). A one-
140 series cluster in Sweden (Glomma) also is clearly affected by snow melt and rain-on-snow events (Bøe
141 et al., 2006). The series are shown in Fig. S43, but not further studied in relation to atmospheric
142 processes. Our final selection, shown in Fig. 3, comprises a set of 39 streamflow series, aggregated
143 into eight clusters with areas of ca. 50,000-100,000 km². The clusters are spatially coherent, internally
144 consistent with respect to seasonality and heavy precipitation regime, and internally homogeneous
145 with respect to time evolution (exceptions are Southern England, where the only two long series

disagreed, and the Danube, where time evolution is less homogeneous, ~~and perhaps Central Germany where all series agree closely except for the Aller~~). The clusters represent Southern England, Southern Norway, the Rhône, the Alpine Rhine, the Lower Rhine, Central Germany, the Elbe, and the Danube.

Seasonality is an important factor to consider as it is characteristic for a given region. Furthermore, the relevance of atmospheric process changes in the course of the year. Winter events tend to be related to different circulation patterns (e.g., zonal flow) than summer events (Stucki et al. 2021). Moreover, the role of convection is stronger in summer. In the following we will therefore perform all analyses for annual data as well as for annual series restricted to flood seasons, defined as May to October (for clusters Upper Rhine and Danube) and November to April (all other clusters). This partitioning captures the seasonal flood characteristics as well as the seasonal differences in atmospheric processes and it still ensures an adequate sample size.

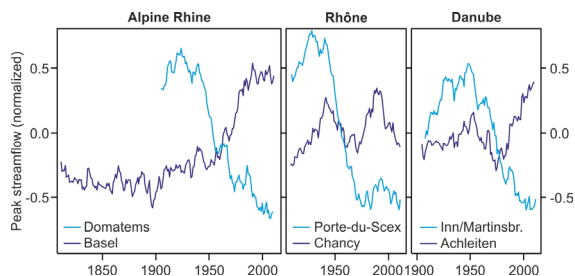


Fig. 2. Normalized smoothed streamflow series for the three Alpine regions. In each region an upstream catchment (mean altitude >2000 m asl, light blue) and streamflow series downstream from the same river system (dark blue) is shown. All series are smoothed with a 30-yr moving average.

2.3. Atmospheric and climate data

The focus of the paper is on the atmospheric contribution to flood intensity. However, studying atmospheric circulation 200 years back in time with a focus on extreme weather events is challenging. To compensate for potential deficiencies of long-term data sets and to obtain more robust results, we use multiple atmospheric data sets that are partly independent and are based on different methods.

The dynamical reanalysis 20CRv3 (Slivinski et al., 2019) provides 3-hourly, 3-dimensional, global atmospheric data back to 1806. 20CRv3 assimilates only surface pressure observations into an atmospheric model with prescribed sea-surface temperatures, sea-ice concentration, and radiative forcings. It consists of 80 equally likely members. All analyses shown here were performed for each member to obtain a physically plausible range of realisations. We extracted one grid point per region (crosses in Fig. 4; selected from the 1x1° grid such as to best represent atmospheric processes relevant for the region; note that we preferred point data, as the Rx5day data also are point data). The reanalysis allows calculating specific diagnostics, such as moisture flux convergence, at a relatively

Formatted: Font: 11 pt, English (United Kingdom)

Formatted: Font: 11 pt, English (United Kingdom)

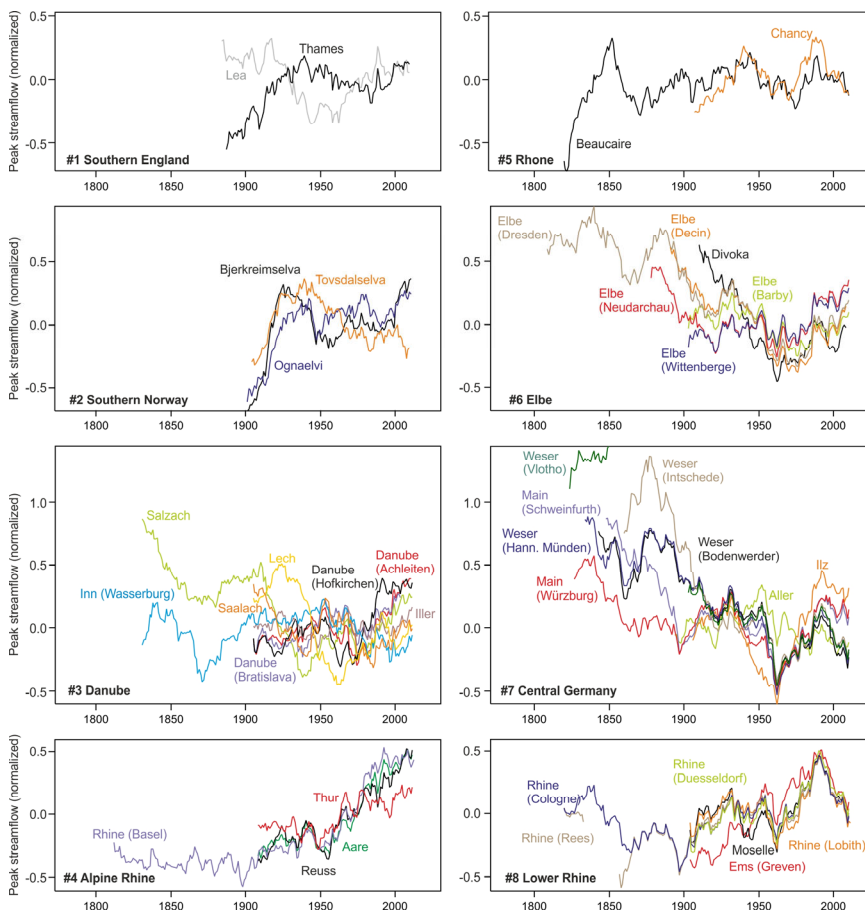
Formatted: Font: 11 pt, English (United Kingdom)

Formatted: Font: 11 pt, English (United Kingdom)

Formatted: English (United Kingdom)

Formatted: Space After: 6 pt

176 high resolution. However, the quality of 20CRv3 varies in time and space, particularly during the 19th
 177 century. The data prior to 1836 are less well evaluated and have a larger uncertainty (Slivinski et al.,
 178 2021). We always show the ensemble mean and ± 1 ensemble standard deviations.
 179 The second data set consists of daily weather types. Floods occur during specific weather patterns with
 180 similar hydro-meteorological characteristics (Stucki et al., 2012) and thus weather type classifications
 181 can be useful to study atmospheric contributions to floods. We use the Swiss CAP7 weather types
 182 back to 1763 (Cluster Analysis of Principal Components, Schwander et al., 2017) which is based on
 183 daily meteorological data from Europe, some of which overlap with 20CRv3.



184
 185 **Fig. 3.** Normalized smoothed streamflow series for all series in all eight clusters. All series are smoothed with a
 186 30-yr moving average.

187 The third data set is the updated global atmospheric paleo-reanalysis EKF400v2 covering the last 400
 188 years (Franke et al., 2020; Valler et al., 2021). EKF400v2 provides monthly global 3-dimensional
 189 reconstructions from an offline assimilation. While there is a small overlap in input data with 20CRv3

190 (some of the pressure series), EKF400v2 mainly assimilates other data (temperature, precipitation,
191 documentary data, tree-rings). However, unlike for the other two data sets, ~~EKF400v2 is we have not~~
192 ~~available at~~ daily resolution. We use the monthly values to analyse seasonal precipitation and 500 hPa
193 geopotential height (GPH).

194 For comparison with climate model data, we analyse monthly precipitation also directly in station data
195 (Peterson and Vose, 1997; Alexander and Jones, 2001; Murphy et al., 2018) and in the observation-
196 based gridded product HISTALP (Efthymiadis et al., 2006), which also includes temperature (note that
197 these data were assimilated into EKF400v2).

198

199 2.4. Flood probability index

200 Based on the weather types, we define a Flood Probability Index (FPI see below), which characterizes
201 a season or year based on sequences of weather types. To calibrate the index we need daily streamflow
202 series, which are available ~~for~~ only for the Rhine (Basel) and Rhône (Beaucaire). We calculate it
203 separately for the warm season (May to October, for Basel) and cold season (November to April,
204 Beaucaire) in order to analyse the seasonally-varying relation of weather types with temperature
205 anomalies. The calculation of the FPI is based on Quinn and Wilby (2013) and is performed exactly as
206 in Brönnimann et al (2019). We first determined the 98th percentile of daily streamflow within the
207 respective seasonal window and marked all days above this percentile as extreme events. Events
208 separated by 3 or fewer days were combined to ensure independence, and from each sequence of
209 marked days only the day of the maximum was kept. For each weather type we then calculated the
210 fraction of days coinciding with a flood event relative to all days of that type. Then we assigned this
211 number to each day of that weather type. This was repeated for different lead times up to 5 days such
212 that the weather on preceding days is also considered, ~~and~~ ~~lead times 5 to 0 were weighted as in~~
213 ~~Brönnimann et al. (2019)~~ 1/16, 1/8, 3/16, 1/4, 1/4, and 1/8. This window length and weighting was
214 taken from a previous study (Brönnimann et al., 2019) and was based on analyses of daily discharge,
215 precipitation, and water flux convergence on the preceding days. This procedure yields an FPI for each
216 day in the past (note that the index was calibrated in the data after 1900, but calculated back to 1763).
217 The 75th percentile of this index calculated for each season was then chosen as an indicator of flood
218 probability (for details see Brönnimann et al., 2019).

219

220 2.6. Water flux convergence

221 Atmospheric circulation was furthermore analysed in terms of advection and convection of moist air.
222 We calculated a simplified measure of moisture flux convergence in which 850 hPa horizontal wind is
223 multiplied with precipitable water, termed water flux convergence in the following. This was
224 calculated for each of the 80 ensemble members of 20CRv3 and each 3-hour interval. In this analysis
225 we use the annual maximum 5-day average, CONV5d (analog to Rx5day; different windows from 3

226 hours to 10 days gave very similar results). All series were smoothed with a 30-year moving average
 227 and finally the members were averaged. CONV5d indicates intense moisture transport and
 228 precipitation.

229 Based on the 3-hourly values feeding in to the maximum 5-day value, we decomposed CONV5d into
 230 its contributions as follows (overbar denotes the average over the entire period (1806-2015), primes
 231 denote deviations therefrom, q denotes precipitable water, \vec{v} is the wind vector):

$$\begin{aligned}
 & -\vec{v} \cdot \left((\bar{q} + q') \cdot (\vec{v} + \vec{v}') \right) = \\
 & -\bar{q} \cdot \left(\frac{\partial \bar{u}}{\partial x} + \frac{\partial \bar{v}}{\partial y} \right) - \bar{u} \cdot \frac{\partial \bar{q}}{\partial x} - \bar{v} \cdot \frac{\partial \bar{q}}{\partial y} \\
 & -\bar{q} \cdot \left(\frac{\partial u'}{\partial x} + \frac{\partial v'}{\partial y} \right) - u' \cdot \frac{\partial \bar{q}}{\partial x} - v' \cdot \frac{\partial \bar{q}}{\partial y} \\
 & -q' \cdot \left(\frac{\partial \bar{u}}{\partial x} + \frac{\partial \bar{v}}{\partial y} \right) - \bar{u} \cdot \frac{\partial q'}{\partial x} - \bar{v} \cdot \frac{\partial q'}{\partial y} \\
 & -q' \cdot \left(\frac{\partial u'}{\partial x} + \frac{\partial v'}{\partial y} \right) - u' \cdot \frac{\partial q'}{\partial x} - v' \cdot \frac{\partial q'}{\partial y}
 \end{aligned}$$

232
 233 This decomposition results in four groups of three terms. The first three terms on the right hand side
 234 (second line) indicate the contribution by the mean flow, the next three terms (third line) the
 235 contribution by changes in circulation (while keeping moisture constant), the next three terms measure
 236 the contribution by changes in precipitable water (while keeping the circulation constant) and the last
 237 three terms describe the interaction of circulation and moisture changes.

238

239 2.7. Model simulations

240 To test the effect of sea-surface temperature and external forcing on multidecadal variations of
 241 atmospheric circulation, we used the global atmospheric model ECHAM6 (Giorgetta et al., 2013). It
 242 was run in the standard configuration T63L47 for the years 1851-2015. The spatial resolution
 243 corresponds to ca. 1.9°. In total 31 members were produced using different initial conditions as well as
 244 different sea-surface temperatures (obtained by sampling from the ten members in HadISST2); only
 245 one realization was available for sea ice (Titchner and Rayner, 2014). All other forcings (land surface,
 246 volcanic aerosols, tropospheric aerosols, and greenhouse gas concentrations) followed the
 247 [Paleoclimate Modelling Intercomparison Project \(PMIP\)](#) protocol (Jungclaus et al., 2017). Ensembles
 248 with individual forcings are not available.

249

250 3. Results and Discussion

251 3.1. Annual peak streamflow

252 The longest 14 series show that extreme floods occurred in the 19th century, particularly in the Elbe,
 253 Weser, and Main catchments, but also Salzach and Rhône show high peaks. Conversely, apart from

254 floods in 1946 (Weser) and 1947 (Lea, Thames, Main), the period ca. 1940 to 1970 exhibits fewer
255 spikes. However, the rivers exhibit different streamflow regimes and flood seasonalities (Fig. S2). The
256 upper (Alpine) catchments of Rhine and Danube exhibit their annual maximum streamflow typically
257 during the warm season, most other catchments during the cold season. After normalizing, the “cold
258 season” and “warm season” rivers were therefore averaged separately and the series were smoothed in
259 Fig. 1b. Likewise, all further analyses were performed for annual series as well as for flood seasons
260 (i.e., Nov-Apr for “cold season” flood rivers and May-Oct for “warm season” flood rivers). Note that
261 throughout the paper, a 30-yr moving average was used for visualisation, where at least 20 values must
262 be available. For averaging regions we require that half of the regions have available data; only when
263 averaging within regions we did not require a minimum as the chosen clusters were largely
264 homogeneous such that the drop-out of a series will not have a large effect.

265 These aggregated curves show additional features. ~~such as a~~ less pronounced peaks for cold-season
266 flood rivers are found in the 1870s and the early 20th century. Based on peaks on the cold-season
267 series, three 30-yr periods were selected for further investigation: 1827-1856 (primary maximum),
268 1949-1978 (primary minimum), and 1919-1948 (local maximum at a time when ; interesting as the
269 warm-season series exhibit low values). While numerous non-climatic factors (e.g., changes in the
270 stream network and land use) contribute to long term trends or may induce step changes (e.g., Hingray
271 et al. 2010), multidecadal variability is less influenced by such changes (note that the Rhine series was
272 corrected for two such changes) and hence climatic conditions are analysed.

273 Our findings of increased flood intensities in Central Europe in the 19th century and a decrease in the
274 mid-20th century are confirmed by documentary evidence (Naulet et al., 2005; Wetter et al., 2011;
275 Himmelsbach et al., 2015; Lang et al., 2016). A recent, comprehensive study based on documentary
276 data and a three-class flood magnitude index (Blöschl et al., 2020) found coherent flood phases in the
277 mid-19th century in Central and Southern Europe, in the early 20th century in northwestern Europe, and
278 in recent decades in Central and Western Europe, although this is not the case for each individual river
279 (Glaser et al., 2010).

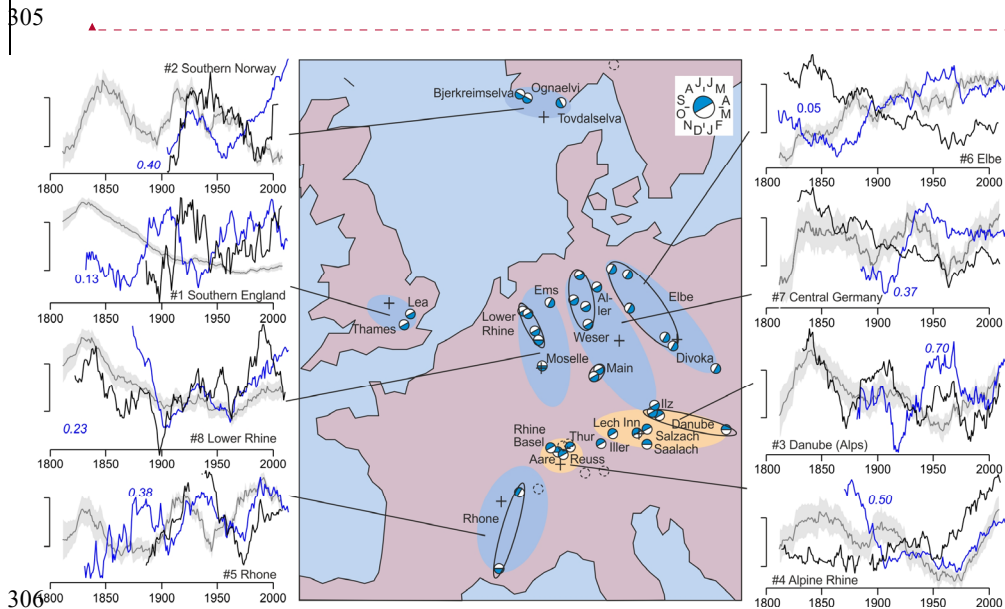
280 Our aggregation into eight regions retains the main phases of flood intensity but adds spatial
281 information. This is shown for annual time series (Fig. S4) as well as for flood seasons (Fig. 4). High
282 peak streamflow occurred in Central Europe in the 19th century, in Central and Western Europe in the
283 early 20th century, low peak streamflow in all regions after 1950. Since 1970 peak streamflow has
284 increased, although not everywhere, and some series (not only those influenced by snow) show a
285 decline at the beginning of the 21st century.

286 For comparison with Blöschl et al. (2020), we add the interpolated and smoothed series calculated
287 from their data and code to Fig. S4S5. Correlations (at 4-yr aggregation, corresponding to the voxel
288 size in Blöschl et al. (2020)) with peak streamflow (numbers in Fig. 4) are between 0.4 and 0.52
289 except for Southern England around or below 0.4, statistically significant (t-test, p<0.05) for the

Formatted: English (United Kingdom)

290 regions Southern Norway, Upper Rhine, Rhone, and Elbe. Obviously, the comparability of
 291 measurement-based versus document-based evidence is limited. For instance, analysed statistics differ
 292 (annual maxima versus indexed extremes), the series measure different aspects of flood (streamflow
 293 versus documented flood intensity) and there is large river-to-river variability. Yet, the flood-rich
 294 decades in the middle and late 19th century in Central Europe, in the early 20th century in Northwestern
 295 Europe, the Europe-wide flood-poor period after 1950, and the recent increase in flood intensity are
 296 salient features of all analyses. This becomes clear when aggregating the series spatially into
 297 Northwestern Europe (UK and Southern Norway) and Central Europe (all other regions) and
 298 smoothing the Blöschl data for better comparability with the 30-yr smoothed streamflow (see Fig. S5).
 299 Hence, the regional characteristics are consistent with the documentary evidence on a climatological
 300 scale, and the fact that corresponding periods of more and less frequent floods are found with both
 301 methods opens the door for the following analyses.

302 In the following, we show results only for the seasonal series (results for the annual series are similar).
 303 Note that flood seasons capture ca. 80% of peak streamflow events, and flood intensities are ca. 8%
 304 higher than on out-of-season floods.



307 **Figure 4.** Regionally averaged (coloured ellipses; black ellipses indicate same river) series of normalized peak
 308 streamflow (black), Rx5day (blue, the number indicates its correlations with peak streamflow at 4-yr aggregation,
 309 *italics indicates p<0.05*) and CONV5d during the flood season from 20CRv3 at locations of crosses (grey, shading
 310 indicates the ensemble standard deviation), standardized and subsequently smoothed with a 30-yr moving
 311 average (scale bars range from -0.5 to +0.5). Regions are colour-coded according to the predominance of cold
 312 (blue; Nov-Apr) or warm season floods (orange; May-Oct). The blue part of the white-blue circle for each river

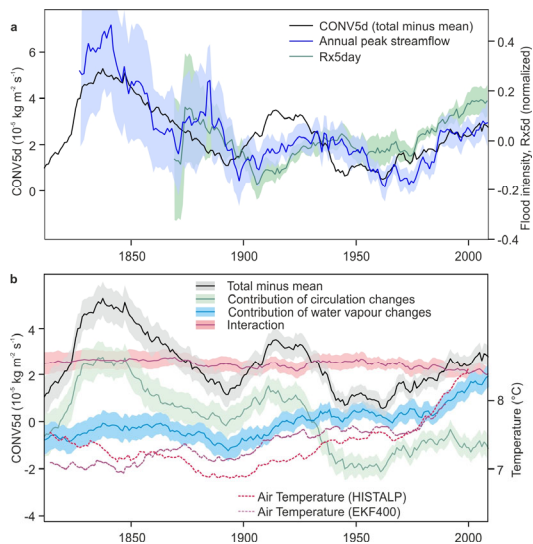
Formatted: English (United Kingdom)

313 indicates the 6-month period with highest flood frequency). Dashed circles: Streamflow series excluded because
314 of likely influence of snow melt, or hydropower dams or other hydraulic constructions on trends.

315 3.2. Atmospheric influences and the role of circulation and water vapour changes

316 First, we analysed the relation between flood intensity and with precipitation. In most regions, flood
317 intensities are statistically related to Rx5day. Correlations (Fig. 4 and S5, again-calculated for 4-yr
318 averages for consistency from annual data) vary greatly (between 0.05 and 0.7), but are significant (t-
319 test, $p < 0.05$) for six regions are 0.21 to 0.57. Note that a high correlation is not necessarily expected on
320 a year-to-year scale as Rx5day events often do not occur together with annual peak streamflow. In
321 winter flood regions, for instance, Rx5day occurs predominantly in summer, whereas peak streamflow
322 occurs predominantly in winter, hence a winter series is correlated with a summer series.
323 Hence Nevertheless, years with high peak stream flow coincide with years with high maximum 5-day
324 precipitation, although the association is not very strong and one needs to keep in mind that flood
325 intensity is not purely atmospherically driven. -Note also that neither peak stream flow (except for
326 Rhine, Basel) nor Rx5day are based on homogenised data series.

327 Next, we analysed atmospheric influences on the multidecadal variability of peak stream flow using
328 the diagnostics defined in Sect. 2. The CONV5d series (grey lines and shading in Fig. 4; for
329 visualization they were standardized prior to filtering) exhibit multidecadal variations with maximum
330 convergence in the 19th and early 20th century and minimum convergence around 1950, although the
331 pattern differs from region to region. They are in general agreement with the maximum streamflow
332 curves for several regions (e.g., Rhône, Lower Rhine, Central Germany, Danube), while in other
333 regions the agreement is worse. Similarly as for Rx5day, CONV5d is less reliable in the early years,
334 prior to ca. 1836. The steep increase in these years therefore cannot be assessed.



335

336 **Figure 5. a** Average of regional averages of annual maxima of peak streamflow, Rx5day, and CONV5d. Shading
337 indicates ± 1 standard error. **b** Contributions to CONV5d from circulation changes, water vapour changes, and
338 their interaction. Shading indicates ± 1 standard deviation of the ensemble. Dashed curves show annual mean
339 temperature from HISTALP and EKF400. All curves are smoothed with a 30-yr moving average.

340 While all individual indicators (flood intensity, Rx5day, CONV5d) have uncertainties that are
341 particularly large in the early decades, there are also clear similarities. A further aggregation reveals
342 the common low-frequency variability even more distinctly. When averaging all three indicators
343 across all eight regions (Fig. 5), we find a close similarity after around 1870. All series show the
344 recent increase, the minimum in the 1960s, a peak around the 1930s, and a minimum around 1900, as
345 already noted in Fig. 1. Flood intensity and CONV5d also show a peak in the 1840s, which is however
346 not seen in the (sparse) Rx5day data. The association between the three series is further supported by
347 cross-wavelet analyses (Fig. S6), which shows significant relations at time scales longer than ca. 30
348 years.

349 Thus, despite the uncertainties, we can use these indicators to trace the atmospheric impacts on the
350 multidecadal variability in flood intensity. The atmospheric processes, in turn, can be partitioned into
351 contributing processes as described in Sect. 2. Figure 5b shows the contributions from circulation
352 changes, from water vapour changes, and from their interaction. The interaction term is negative with
353 only small changes over time. The contribution from circulation changes (green line) dominates and
354 shows all main features found in CONV5d. However, the long term trend differs. This is due to
355 changes in water vapour (blue line). The contribution of water vapour changes shows a two-step
356 increase after 1900.

357 An analysis of linear trends in the unsmoothed series since 1963, the minimum in flood intensity,
358 reveals an increase in CONV5d ($4.04 \times 10^{-7} \text{ kg m}^{-2} \text{ s}^{-1} \text{ yr}^{-1}$, which is not statistically significant), no
359 trend in the contribution of atmospheric circulation changes, but a highly significant increase in the
360 contribution of water vapour changes ($6.13 \times 10^{-7} \text{ kg m}^{-2} \text{ s}^{-1} \text{ yr}^{-1}$).

361 The contribution of water vapour changes depends on temperature through the Clausius-Clapeyron
362 relation. To illustrate this relation, annual mean temperature in HISTALP (Efthymiadis et al 2006), the
363 longest gridded observational data set, and in EKF400v2 for the same regions are plotted such that 1
364 °C corresponds to $0.46 \cdot 10^{-5} \text{ kg m}^{-2} \text{ s}^{-1}$. This is equivalent to a 6.5% change in CONV5d, the number
365 expected following the Clausius-Clapeyron relation if annual maxima would follow the annual
366 average trend (saturation can be assumed for annual maximum moisture convergence). After around
367 1900, the general pattern and amplitude of the contribution of water vapour changes is consistent with
368 an increased intensity of heavy precipitation in a warming atmosphere, although the amplitude of the
369 CONV5d increase is somewhat smaller than that of the scaled temperature increase.

370 In fact, this might help to explain the varying relation between temperature and floods over time:
371 Palaeoclimate studies (Stewart et al 2011, Glur et al 2013, Wilhelm et al. 2021), particularly from the

Formatted: Superscript

Formatted: Superscript

Formatted: Superscript

Formatted: Superscript

372 northern Alps, suggest that past flood-rich periods coincided with cool periods, while climate
373 projections suggest that with global warming, flood occurrence may increase in certain regions.

374 Although palaeoclimate studies often are based on small catchments, target a longer return period and
375 a low-frequency variability scale that is longer than decades as in this study, it is nevertheless
376 interesting to analyse the relation between temperature and floods on a multidecadal scale.

377 To analyse the role of circulation for temperature, we used the FPI index for the Rhône and Rhine,
378 which was calculated specifically for the corresponding flood seasons (Nov-Apr for the Rhône, May-
379 Oct for the Rhine). This index measures the frequency of flood-prone weather types, to which cyclonic
380 weather types contribute very strongly. As a consistency test, the smoothed curves (Fig. 6a) show high
381 values in the 19th and early 20th century and a decrease after ca. 1950; further analyses of the FPI index
382 for Basel are shown in Brönnimann et al. (2019). For the following analysis we used the unsmoothed,
383 but detrended FPI indices, onto which we regressed the detrended temperature fields of the
384 corresponding seasons (Fig. 6b). For the Rhine, which is mostly affected by summer floods, flood
385 prone seasons are typically cold. Conversely, for the Rhône, with typically winter floods, flood-prone
386 seasons are warmer than average in the lowland, but colder than average at higher altitudes. Both are
387 consistent with a predominance of cyclonic weather types over Switzerland: They bring colder than
388 average weather in summer, but warmer than average in winter except at high altitudes, which
389 normally, but not during cyclonic weather types, are ~~often~~ above an inversion.

390 This means that from the contribution of circulation alone, flood-rich periods in summer-flood regions
391 and generally in the Alps are expected to be cool. This is not the case after 1980, when the partitioning
392 (Fig. 5b) shows a growing contribution of water vapour increase whereas the contribution of
393 circulation changes is constant (and the FPI is low, Fig. 6a). Warming phases (also in the past) rather
394 directly lead to an increase in CONV5d, but warming may be driven by atmospheric circulation
395 changes that decrease CONV5d, or it may be driven by other forcings in which case atmospheric
396 circulation does not counteract the increase in CONV5d.

397

398 *3.4. Regional differences in circulation effects*

399 Circulation changes had regionally different imprints in different times. Recall that 1827-1856 was
400 flood-rich in Central Europe (year-round), 1919-1948 was flood-rich in northern and western Europe
401 (cold season), 1949-1978 was flood-poor across Europe (year-round, Fig. 1). The contribution of
402 circulation changes to CONV5d (shown in Fig. 7 for each region) is consistent with this result. Some
403 regions show an almost opposite behaviour to each other. For instance, in the mid 19th century,
404 circulation changes contributed to high CONV5d in Southern Norway but to relatively low values in
405 the Rhône catchment, whereas the opposite was the case in the second half of the 20th century (Fig. 7).

406 While the contribution of circulation differs from region to region, the contribution from water
407 vapour changes is more uniform and shows an increase in all regions.

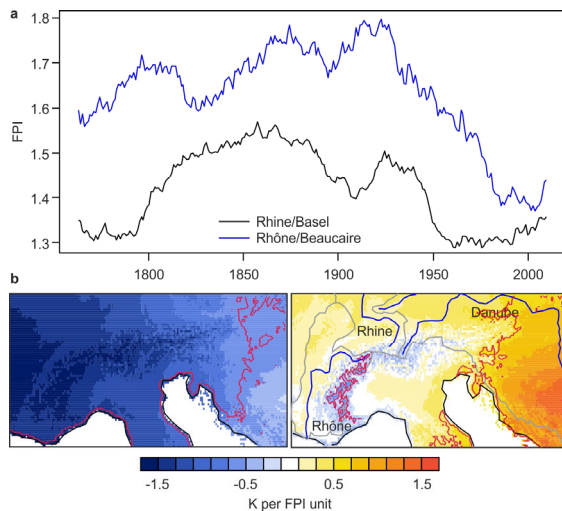


Figure 6. a. FPI index for the Rhine in Basel (May-Oct) and the Rhône in Beaucaire (Nov-Apr), smoothed with a 30-yr moving average. **b.** Regression map of detrended seasonal (May-Oct and Feb-Apr, respectively) mean temperature in HISTALP onto the corresponding (detrended) FPI indices. Red lines indicate significant ($p < 0.05$) coefficients.

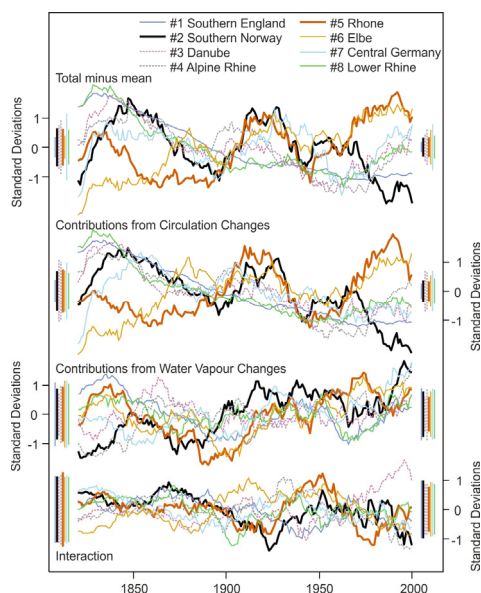
Formatted: Font: Bold

Formatted: Font: Bold

To test whether these spatial differences due to atmospheric circulation are reflected in the seasonal mean large-scale flow, we analysed (Fig. 8) 30-yr averages of seasonal mean anomalies in precipitation and 500 hPa GPH in EKF400v2 and observations (Peterson and Vose, 1997; Alexander et al., 2001; Murphy et al., 2018). In terms of seasonal mean precipitation, the cold seasons 1827-1856 and 1949-1978 show a rather mixed signal. Although not inconsistent with the observed multidecadal flood intensity, one would probably not address these periods as flood-rich and flood-poor, respectively, based only on seasonal mean precipitation (note that Blöschl et al. (2020) define a flood period in 1840-1872; corresponding plots exhibit similar patterns as for 1827-1856; Fig. SSS7).

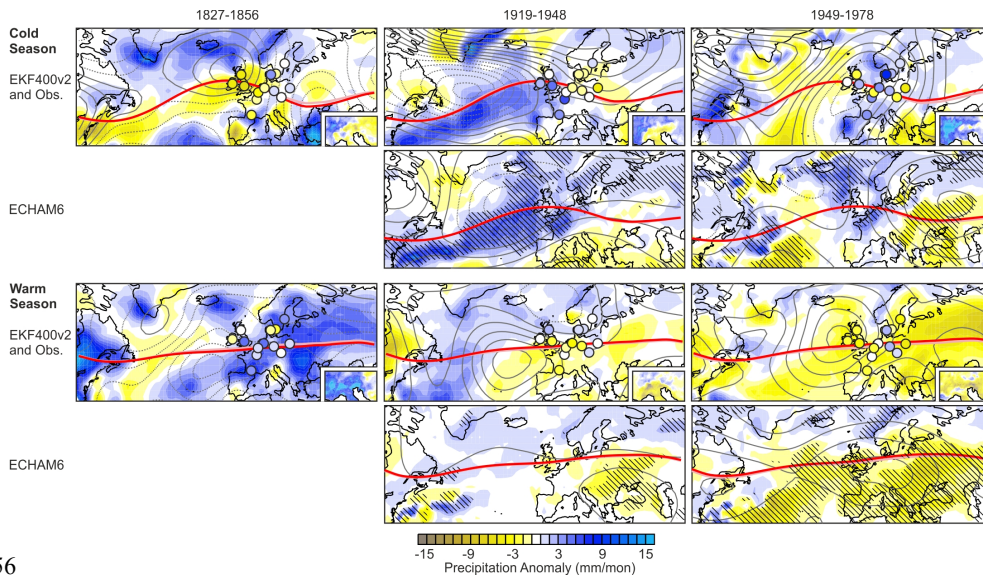
The period 1827-1856 (cold season) shows a pressure pattern that is similar to a negative mode of the North Atlantic Oscillation or East Atlantic Pattern, but with the positive pressure anomaly displaced southeast of Iceland. Seasonal mean precipitation (both in EKF400v2 and station data) shows a mixed signal; with slight increases in the Rhône catchment, Central Europe, and Southern Norway, but drying over England. The warm season shows negative anomalies of 500 hPa GPH over the entire continent, accompanied by increased rainfall, which is consistent with frequent flood-prone weather.

The 1919-1948 cold season average shows negative 500 hPa GPH anomalies over the Atlantic and increased precipitation over Western Europe, which agrees with the increased flood intensity in this region. The clearest signal is found for the flood-poor period 1949-1978 in the warm season. The analysis shows pronounced drying and positive anomalies of 500 hPa GPH. The start of this period, which coincided with massive droughts (e.g., Brazdil et al., 2016) was accompanied by a poleward shifted subtropical jet (Brönnimann et al., 2015).



433
 434 **Figure 7.** CONV5d (total minus mean) and contributions to it from circulation changes, water vapour changes,
 435 and their interaction for each of the eight regions (ensemble mean). All series were standardized and smoothed
 436 with a 30-yr moving average. Coloured bars indicate ± 1 one ensemble standard deviation at the beginning and
 437 end of the period (the change inbetween is close to linear).

438 We further addressed the underlying causes of multidecadal anomalies by analysing, in the same way
 439 as EKF400v2, an ensemble of 31 simulations with the ECHAM6 atmospheric model starting in 1851
 440 (the 1827-1856 period cannot be analysed). The precipitation anomalies and the broad features of
 441 GPH anomalies found in EKF400v2 are rather well reproduced for the 1919-1948 and 1949-1978
 442 periods, both cold and warm seasons (for 1840-1872 see Fig. S5). For instance, for the cold season, the
 443 negative GPH anomalies over the North Atlantic in 1918-1948 and the zonal pattern of low GPH over
 444 the eastern North Atlantic and high GPH over Russia in 1949-1978 agree well. The wet conditions in
 445 western Europe in 1919-1948 in winter and the dry conditions in 1949-1978 in summer are highly
 446 significant in the atmospheric model simulations. The latter is arguably the most significant feature in
 447 the model analysis. Although this analysis concerns only changes in the seasonal means, not in
 448 extremes, it shows that atmospheric model simulations forced with, among other factors, sea-surface
 449 temperatures are able to reproduce some characteristic features of atmospheric circulation changes.
 450 However, the seasonal mean circulation and precipitation describes the flood conditions only to a
 451 limited extent (see Zanchettin et al., 2019, for the role of Atlantic sea-surface temperature variability
 452 for floods). Note, also, that also EKF400v2, despite the large number of observations assimilated, is
 453 dependent on sea-surface temperature input to the underlying model. Overall, the model simulations
 454 suggest that part of the multidecadal variability can be reproduced from model boundary conditions
 455 (note that in addition to sea-surface temperature, they also encompass external forcings).



456
 457 **Figure 8.** Simulated atmospheric circulation and precipitation. Anomalies (with respect to 1851-1950) of
 458 precipitation (colours) and 500 hPa GPH (contour distance 2 gpm centered around zero, dashed contours
 459 indicate negative numbers) in the 30-yr periods 1827-1856, 1919-1948, and 1949-1978 in the EKF400v2
 460 reconstruction (ensemble mean), observations (insets: HISTALP; circles: GHCN), and ECHAM6 simulations
 461 (hatching denotes 95% significance of precipitation anomalies, calculated from the 30-year averages of the 31
 462 members using a one-sample t-test). Thick red lines show the GPH contour 5450 gpm (cold season) or 5650 gpm
 463 (warm season; light pink: same for 1851-1950).

464

465 **5. Conclusions**

466 Long time series of annual peak streamflow in Western and Central Europe exhibit substantial
 467 multidecadal variability, consistent with previous work by other authors. Flood-rich phases occurred in
 468 the 19th century in several regions, in the early 20th century in western and northern Europe, and since
 469 the 1980s, while a flood-poor period occurred after the second world war. The flood variability is in
 470 line with observed changes in Rx5day (except in the mid-19th century, which however could be due to
 471 a lower data quality).

472 Annual peak atmospheric water flux convergence in a reanalysis also shows the same pattern of
 473 multidecadal variability as flood intensity and Rx5day, and this is further supported by an indicator
 474 based on weather types. Although the uncertainties in each data set are large, results are robust and
 475 show the same main phases of low-frequency variability. The reanalysis data allow a more physical
 476 interpretation. Partitioning the atmospheric water flux convergence into contributions from circulation
 477 and water vapour changes, we find that peak streamflow of European rivers from around 1820 to 1980
 478 was largely forced by atmospheric circulation changes. In contrast, the recent increase in moisture flux

479 convergence was to a larger part driven by increasing atmospheric moisture due to climate change.
480 This might contribute to explaining why in the past, flood-rich periods coincided with cold periods
481 (particularly in summer-flood regions such as the northern Alps, to which many proxy studies refer)
482 while more floods may be possible in Europe in a future, warming climate. Note, however, that
483 paleoclimatic studies often address longer time scales, smaller catchments, and longer return periods
484 than are used in this study.

485 Changes in seasonal mean atmospheric circulation partly mirror the changes in flood intensity
486 changes. Important features of these changes are reproduced in atmospheric model simulations,
487 indicating that oceanic forcing might play a role. This is specifically the case for the dry and flood-
488 poor summers 1949-1978.

489 The thermodynamic effect is likely to increase further. The floodings in Central and Western Europe
490 the summer of 2021 fit into the picture of a stronger thermodynamic contribution. However, flood
491 projections in Europe under different emission scenarios remain unclear (Kundzewicz et al., 2017), as
492 several sources of uncertainties have to be considered (climate models, downscaling, hydrological
493 models) and projections for flood intensity (e.g. Roudier et al., 2016), frequency (e.g. Giuntoli et al.,
494 2015) or both (e.g. Alfieri et al., 2015) in European rivers vary.

495

496 *Acknowledgements:* This work was supported by Swiss National Science Foundation project WeaR (188701),
497 and by the European Commission (ERC Grant PALAEO-RA, 787574). Simulations were performed at the Swiss
498 National Supercomputing Centre CSCS. Support for the Twentieth Century Reanalysis Project version 3 dataset
499 is provided by the U.S. Department of Energy, Office of Science Biological and Environmental Research (BER),
500 by the National Oceanic and Atmospheric Administration Climate Program Office, and by the NOAA Physical
501 Sciences Laboratory. We acknowledge the data providers in the ECA&D project.

502 **References**

- 503 Alexander, L. V. and Jones, P. D.: Updated precipitation series for the UK and discussion of recent extremes, Atmos. Sci.
504 Lett. doi:101006/asle20010025, 2001.
- 505 Alfieri, L., Burek, P., Feyen, L. and Forzieri, G.: Global warming increases the frequency of river floods in Europe, Hydrol.
506 Earth Syst. Sci., 19, 2247–2260, 2015.
- 507 Alfieri, L., Bisselink, B., Dottori, F., Naumann, G., de Roo, A., Salamon, P., Wyser, K. and Feyen, L.: Global projections of
508 river flood risk in a warmer world. Earth's Future, 5, 171-182, 2017.
- 509 Blöschl, G. et al.: Current flood-rich period exceptional compared to past 500 years in Europe Nature, 583, 522-524, 2020.
- 510 Bøe, A.-G., Dahl, S. O., Lie, Ø. and Nesje, A.: Holocene river floods in the upper Glomma catchment, southern Norway: a
511 high-resolution multiproxy record from lacustrine sediments, The Holocene, 16, 445-455, 2006.
- 512 Botter, G., Basso, S., Rodriguez-Iturbe, I. and Rinaldo, A.: Resilience of river flow regimes, Proc. Natl. Acad. Sci., 110,
513 12925-12930, 2013.
- 514 Brázdil, R., Pfister, C., Wanner, H., von Storch, H. and Luterbacher, J.: Historical climatology in Europe – the state of the art,
515 Clim. Change., 70, 363–430, 2005.
- 516 Brázdil, R. et al.: The Central European drought of 1947: causes and consequences, with particular reference to the Czech
517 Lands, Clim. Res., 70, 161-178, 2016.
- 518 Brönnimann, S. et al.: Southward shift of the Northern tropical belt from 1945 to 1980, Nat. Geosci., 8, 969-974, 2015.

519 Brönnimann, S. et al.: Causes for increased flood frequency in central Europe in the 19th century, *Clim. Past.*, 15, 1395–
520 1409, 2019.

521 Efthymiadis, D. et al.: Construction of a 10-min-gridded precipitation data set for the Greater Alpine Region for 1800–2003,
522 *J. Geophys. Res.*, 111, D01105, 2006.

523 Engeland, K. et al.: New flood frequency estimates from the largest river in Norway based on the combination of short and
524 long time series, *Hydrol. Earth Syst. Sci.*, 24, 5595–5619, 2020.

525 Franke, J., Valler, V., Brugnara, Y. and Brönnimann, S.: Ensemble Kalman Fitting Paleo-Reanalysis Version 2 (EKF400_v2)
526 World Data Center for Climate (WDCC) at DKRZ https://doi.org/10.26050/WDCC/EKF400_v2, 2020.

527 [Froidevaux, P., Schwanbeck, J., Weingartner, R., Chevalier, C., and Martius, O.: Flood triggering in Switzerland: the role of](#)
528 [daily to monthly preceding precipitation](#), *Hydrol. Earth Syst. Sci.*, 19, 3903–3924, [https://doi.org/10.5194/hess-19-3903-](https://doi.org/10.5194/hess-19-3903-2015)
529 [2015](#), 2015.

530 Giorgetta, M. A. et al.: *The atmospheric general circulation model ECHAM6 - Model description*, Reports on Earth System
531 Science, 135, 2013.

532 Giuntoli, I., Vidal, J.-P., Prudhomme, C. and Hannah, D. M.: Future hydrological extremes: The uncertainty from multiple
533 global climate and global hydrological models, *Earth Syst. Dyn.*, 6, 267–285, 2015.

534 Glaser, R. et al.: Floods in Central Europe since AD 1300 and their regional context, *La Houille Blanche*, 5, 43–49, 2004.

535 Glaser, R. et al.: The variability of European floods since AD 1500, *Clim. Change.*, 101, 235–256, 2010.

536 Glur, L. et al.: Frequent floods in the European Alps coincide with cooler periods of the past 2500 years, *Sci. Rep.*, 3, 2770,
537 2013.

538 Hall, J. et al.: Understanding flood regime changes in Europe: a state-of-the-art assessment, *Hydrol. Earth Syst. Sci.*, 18,
539 2735–2772, 2014.

540 Himmelsbach, I., Glaser, R., Schoenbein, J., Riemann, D. and Martin, B.: Reconstruction of flood events based on
541 documentary data and transnational flood risk analysis of the Upper Rhine and its French and German tributaries since
542 AD 1480, *Hydrol. Earth Syst. Sci.*, 19, 4149–4164, 2015.

543 [Hingray, B., Schaeffli, B., Mezghani, A. and Hamdi, Y.: Signature-based model calibration for hydrological prediction in](#)
544 [mesoscale Alpine catchments](#), *Hydrol. Sci. J.*, 55, 1002–1016, 2010.

545 [IPCC: Summary for Policymakers. In: Climate Change 2021: The Physical Science Basis. Contribution of Working Group I](#)
546 [to the Sixth Assessment Report of the Intergovernmental Panel on Climate Change \[Masson-Delmotte, V. et al. \(eds.\)\].](#)
547 [Cambridge University Press. In Press, 2021.](#)

548 Jacobeit, J., Glaser, R., Luterbacher, J., and Wanner, H.: Links between flood events in Central Europe since AD 1500 and
549 largescale atmospheric circulation modes, *Geophys. Res. Lett.*, 30, 1172–1175, 2003.

550 Jungclaus, J. H. et al.: The PMIP4 contribution to CMIP6 – Part 3: The last millennium scientific objective and experimental
551 design for the PMIP4 past1000 simulations, *Geosci. Model Dev.*, 10, 4005–4033, 2017.

552 Klein Tank, A.M.G. et al.: Daily dataset of 20th-century surface air temperature and precipitation series for the European
553 Climate Assessment, *Int. J. Climatol.*, 22, 1441–1453, 2002.

554 Kundzewicz, V. et al.: Differences in flood hazard projections in Europe – their causes and consequences for decision
555 making, *Hydrol. Sci. J.*, 62, 1–14, 2017.

556 Lang, M., Coeur, D., Audouard, A., Villanova-Oliver, M. and Pène, J.-P.: BDHI: a French national database on historical
557 floods E3S Web Conf 7 04010, 2016.

558 Mudelsee, M., Börngen, M., Tetzlaff, G. and Grünewald, U.: Extreme floods in central Europe over the past 500 years: Role
559 of cyclone pathway “Zugstrasse Vb”, *J. Geophys. Res.*, 109, D23101, 2004

560 Murphy, C. et al.: A 305-year continuous monthly rainfall series for the island of Ireland (1711–2016), *Clim. Past*, 14, 413–
561 440, 2018.

562 Naulet, R. et al.: Flood frequency analysis on the Ardèche river using French documentary sources from the last two
563 centuries, *J. Hydrol.*, 313, 58–78, 2005.

564 Peterson, T. C. and Vose, R. S.: An overview of the Global Historical Climatology Network temperature database, *B. Amer.*
565 [Meteorol. Soc.](#), 78, 2837–2849, 1997.

566 Pfister, C.: Die „Katastrophenlücke“ des 20. Jahrhunderts und der Verlust traditionellen Risikobewusstseins, *Gaia*, 18, 239–
567 246, 2009.

Formatted: German (Germany)

568 Quinn, N. and Wilby, R. L.: Reconstructing multi-decadal variations in fluvial flood risk using atmospheric circulation
569 patterns, *J. Hydrol.*, 487, 109-121, 2013.

570 Roudier, P. et al.: Projections of future floods and hydrological droughts in Europe under a +2°C global warming, *Clim.*
571 *Change*, 135, 341–355, 2016.

572 Schmocker-Fackel, P. and Naef, F.: Changes in flood frequencies in Switzerland since 1500 *Hydr Earth Sys Sci* 14 1581–
573 1594, 2010a

574 Schmocker-Fackel, P. and Naef, F.: More frequent flooding? Changes in flood frequency in Switzerland since 1850, *J.*
575 *Hydrol.*, 381, 1–8, 2010b.

576 Schwander, M. et al.: Reconstruction of Central European daily weather types back to 1763, *Int. J. Climatol.*, 37, 30-44,
577 2017.

578 Slivinski, L. C. et al.: An evaluation of the performance of the 20th Century 1 Reanalysis version 3, *J. Clim.*, 34, 1417–1438,
579 2021.

580 Slivinski, L. C. et al.: Towards a more reliable historical reanalysis: Improvements to the Twentieth Century Reanalysis
581 system, *Q. J. Roy. Meteorol. Soc.*, 145, 2876-2908, 2019.

582 Stewart, M. M., Grosjean, M., Kuglitsch, F. G., Nussbaumer, S. U. and von Gunten, L.: Reconstructions of late Holocene
583 paleofloods and glacier length changes in the Upper Engadine Switzerland (ca 1450 BC–AD 420), *Palaeogeogr.*
584 *Palaeoclimatol.*, 311, 215–223, 2011.

585 Stucki, P. et al.: Five weather patterns and specific precursors characterize extreme floods in Switzerland, *Meteorol. Z.*, 21,
586 531-550, 2012.

587 Summermatter, S.: *Die Überschwemmungen von 1868 in der Schweiz Unmittelbare Reaktion und längerfristige Prävention*
588 *mit näherer Betrachtung des Kantons Wallis*, Nordhausen, T. Bautz, 2005

589 Tarasova, L. et al.: Causative classification of river flood events, *WIREs Water*, 6, e1353, 2019.

590 Titchner, H. A. and Rayner, N. A.: The Met Office Hadley Centre sea ice and sea surface temperature data set version 2: 1
591 Sea ice concentrations, *J. Geophys. Res.*, 119, 2864–2889, 2014.

592 Valler, V., Franke, J., Brugnara, Y. and Brönnimann, S.: An updated global atmospheric paleo-reanalysis covering the last
593 400 years, *Geosc. Data. J.*, doi: 101002/gdj3121, 2021.

594 Vose, et al.: *The Global Historical Climatology Network: Long-term monthly temperature, precipitation, sea level pressure,*
595 *and station pressure data*, Oak Ridge National Laboratory Environmental Sciences Division Publ. 3912, 324 pp, 1992.

596 Wetter, O. et al.: The largest floods in the High Rhine basin since 1268 assessed from documentary and instrumental
597 evidence, *Hydrol. Sci. J.*, 56, 733–758, 2011.

598 Zanchettin, D. et al.: Atlantic origin of asynchronous European interdecadal hydroclimate variability, *Sci. Rep.*, 9, 10998,
599 2019.

600 **Data availability**

601 The GRDC data can be downloaded here: https://www.bafg.de/GRDC/EN/Home/homepage_node.html

602 Flood series on the Rhône river at Beaucaire (1816-2016) is available from: [https://www.plan-](https://www.plan-rhone.fr/publications-131/actualisation-de-lhydrologie-des-crues-du-Rhone-1865.html?cHash=5628938abc287dc9ca390dad7373ae0e)
603 [Rhône.fr/publications-131/actualisation-de-lhydrologie-des-crues-du-Rhône-](https://www.plan-rhone.fr/publications-131/actualisation-de-lhydrologie-des-crues-du-Rhone-1865.html?cHash=5628938abc287dc9ca390dad7373ae0e)
604 [1865.html?cHash=5628938abc287dc9ca390dad7373ae0e](https://www.plan-rhone.fr/publications-131/actualisation-de-lhydrologie-des-crues-du-Rhone-1865.html?cHash=5628938abc287dc9ca390dad7373ae0e)

605 EKF400v2.0 is available from: https://doi.org/10.26050/WDC/EKF400_v2.0, 2020

606 20CRv3 is available here: https://portalnersec.gov/project/20C_Reanalysis/

607 HISTALP is available here: <http://www.zamg.ac.at/histalp/datasets.php>

608 The CAP7 weather types are available from <https://cp.copernicus.org/articles/15/1395/2019/>, the Lamb weather
609 types are available from <https://doi.pangaea.de/10.1594/PANGAEA.896307>

610 **Code availability**

611 The code for the processing of the streamflow data as well as for generating the FPI is attached as supplementary
612 file together with all input data.

613 **Author contributions**

614 SB designed the studies and did most of the analyses and writing. PS processed reanalysis data, JF, VV, and YB
615 provided the EKF400v2 data and helped in the analysis, RH performed the climate model simulations, LCS,
616 GPC and PDS provided the 20CRv3 reanalysis data and interpretation, ML provided the Rhône data and BS
617 assisted in the hydrological analyses. ML and BS assisted in the hydrological interpretations. All authors actively
618 discussed the results and all authors contributed to writing.